Journal of Power Sources 223 (2013) 293–305

Contents lists available at SciVerse ScienceDirect

Journal of Power Sources

journal homepage: www.elsevier.com/locate/jpowsour

Equalization integrated online monitoring of health map and worthiness of replacement for battery pack of electric vehicles

Rohit Ugle [a], Yaoyu Li [b,*], Anoop Dhingra [a]

[a] Department of Mechanical Engineering, University of Wisconsin – Milwaukee, 3200 N. Cramer St., EMS 506, Milwaukee, WI 53211, USA
[b] Department of Mechanical Engineering, University of Texas at Dallas, 800 W. Campbell Rd., EC-38 Richardson, TX 75080, USA

ARTICLE INFO

Article history:
Received 6 July 2012
Received in revised form
7 September 2012
Accepted 23 September 2012
Available online 28 September 2012

Keywords:
Electric vehicle
Battery equalization
Internal resistance
Worthiness of replacement
Subspace identification

ABSTRACT

Ever increasing acceptance of electric vehicles relies on better operation and control of large battery packs. The individual modules in large battery packs cannot have identical characteristics and may degrade differently due to manufacturing variability and other factors. Degraded battery modules waste more power, affecting the performance and economy for the whole battery pack. Also, such impact varies with different trip patterns. It is beneficial if the performance gain can be evaluated online prior to replacing certain battery module regarding to actual driving. In this paper, the research objectives are two-fold. First, we propose an on-line battery module degradation diagnostic scheme using the intrinsic signals of battery module equalization. Without need for additional sensors or offline tests, this scheme is cost-effective for constructing and updating the battery pack "health map" in real time during the vehicle operation. Secondly, based on the derived battery health map, the Worthiness of Replacement (WOR) for certain modules/cells is proposed to evaluate the performance of the battery pack for customer specified trip. Such evaluation index provides a quantitative measure for module replacement and battery pack swapping Simulation study is performed to validate the proposed ideas using an actual driving cycle recorded for a commuting trip.

1. Introduction

Electric vehicles (EV) require large battery packs with high energy and power densities to become a competitive choice of transport. There has been extensive research on battery equalization and management systems for EV [1]. Various battery management systems have been developed to achieve cost-effective and fast voltage equalization, simultaneously with battery state-of-charge (SOC) and health monitoring [2,3]. The inter-module voltage and charge equalization is critical for healthy and efficient operation of large battery pack [4]. Battery equalization can relieve the negative impact of degraded modules, although not reversing the degradation [5]. However, with degraded module(s) present, there is significant power loss during the equalization process due to the increased internal resistance, and such loss is also affected by the driving cycle (or the trip pattern). It is of EV customers' interest to evaluate the (negative) consequences of degraded module(s) and decide if replacement is necessary. The decision of replacement thus relies on a combination of both diagnosis of physical conditions and economical payback. More specifically, one desires to know: 1) how much energy loss would be induced for a specific driving cycle (trip), based on the knowledge of module characteristics within the battery pack, and 2) for the given battery pack, what energy efficiency it would be by replacing certain degraded module or cell with a healthy one. Recently, we have investigated these two issues considering the internal resistance as the primary indicator for battery health [6].

The solution to the first problem can be facilitated via online acquisition of battery health map, and more specifically, the module-wise internal resistance map [7]. In this study, we propose to identify the internal resistances of individual modules via the signals during module equalization process. From the system identification standpoint, this approach takes the driving cycle power demand as input excitation to identify the parameters (i.e. internal resistances) needed for battery health mapping. Without need for any extra sensor, this method has the cost-effective advantage.

For the second issue, this study proposes a quantitative measure for the evaluation of module based replacement, named as the "Worthiness of Replacement" (WOR). For a given driving cycle, the WOR of a specific battery pack is defined as the ratio of the SOC change of the current battery pack to that after replacing certain

* Corresponding author. Tel.: +1 414 791 3318; fax: +1 972 883 4659.
E-mail address: yaoyu.li@utdallas.edu (Y. Li).

0378-7753/$ – see front matter © 2012 Elsevier B.V. All rights reserved.
http://dx.doi.org/10.1016/j.jpowsour.2012.09.083

module with a healthy module of nominal specifications. Any performance evaluation for vehicle powertrain relies on the use of driving cycle. Such evaluation can be performed for standard (e.g. DOE or EPA) driving cycles or any user specified trip (e.g. from onboard GPS) because the driving cycle pattern can strongly affect the power demand profile, and in turn the current flow through the whole battery pack and the equalization currents among the individual modules [8]. Recently, there have been significant efforts in using trip information and modeling to optimize the energy management for HEV (hybrid electric vehicles), PHEV (plug-in hybrid electric vehicles) and EV [9]. In this study, we will evaluate the WOR concept via actual driving cycle data.

The above two aspects of work are validated with an EV model, parameterized like a light-duty delivery vehicle. An example service trip during the morning rush hours is used for illustration, which consists of both local road and freeway road segments. An existing battery equalization strategy is implemented [10], and a subspace identification method is applied to identify the battery module internal resistances via the charging and discharging signals. The battery internal resistance map thus obtained is also SOC dependent, which makes the WOR evaluation more accurate.

The remainder of this paper is organized as follows. The EV and battery models are presented in next section. Section 3 describes the battery module equalization scheme adopted in this study. Then, the subspace identification based internal–resistance estimation is presented in Section 4. Simulation results are presented in Section 5, and the work is concluded in Section 6.

2. Electric vehicle and battery model

2.1. Electric vehicle configuration & modeling

The EV model used for this study is assumed to be driven by a 4-pole, 560 V, permanent magnet synchronous motor (PMSM) with a gearbox transmission. The rated speed is 5000 rpm. There are two different battery pack configuration which will be described in Section 5. The torque limits were set to 140 N-m during driving and 160 N-m during braking, respectively. In order to derive the motor driving torque and motor current, the vehicle propulsion dynamics is needed. Based on the propulsional dynamics, the wheel torque is [11]

$$T_{wh} = (F_{ad} + F_{rr} + F_{acc})r \tag{1}$$

where, $F_{ad} = 1/2\rho AC_d v^2$ is the aerodynamic resistance force, $F_{acc} = Ma$ is the acceleration force, and $F_{rr} = \mu_{rr}Mg$ is the rolling resistance force. M is the vehicle mass and a is the acceleration. μ_{rr} is the rolling resistance coefficient, ρ is the air density, A is the effective frontal area, C_d is the drag coefficient, and v is the vehicle speed. The driving torque at the motor shaft is

$$T_m = \frac{T_{wh}}{G\cdot\eta_g} \tag{2}$$

where, T_m is the motor shaft torque, T_{wh} is the torque at wheels, r is the wheel radius, G is the gear ratio, and η_g is the gear efficiency. In this study, the vehicle parameters are set as follows: $M = 1560$ kg, $G = 11$, $C_d = 0.19$, $\mu_{rr} = 0.0048$, $\eta_g = 0.95$ and $r = 0.3$ m.

2.2. Battery models

It is assumed that battery is the only power source for the simulated EV system, and the lithium-ion battery is assumed. There are two battery models used in this study: one is the simulation model based on detailed battery physics, and the other is a simplified model for subspace system identification based internal resistance estimation.

To develop the virtual plant of electric vehicle propulsion for simulation study, a detailed lithium-ion battery model is adopted from MATLAB Simulink® SimPowerSystem™, which consists of nonlinear time-domain models for charging and discharging processes, respectively [12,13].

For discharging process ($i^* > 0$),

$$E = E_0 - K\cdot\frac{Q}{Q-it}\cdot i^* - K\cdot\frac{Q}{Q-it}\cdot it + A\cdot\exp(-B\cdot it) \tag{3a}$$

For charging process ($i^* < 0$),

$$E = E_0 - K\cdot\frac{Q}{it+0.1*Q}\cdot i^* - K\cdot\frac{Q}{Q-it}\cdot it + A\cdot\exp(-B\cdot it) \tag{3b}$$

where E is no-load voltage, E_0 is constant voltage, K is polarization constant, i^* is the low-frequency current, i is the battery current, it is the extracted capacity, Q is maximum battery capacity, A is exponential voltage and B is exponential capacity.

For the online estimation of battery module internal resistance, a simplified linearized R–C battery model is used. Among the various battery models we adopted a battery model from [14] for internal resistance estimation, as shown in Fig. 1. In the R–C model, C_S and C_L are surface capacitance and bulk capacitance, respectively. R_S, R_L and R_0 are surface resistance, bulk resistance and series resistance, respectively. In general, R_0 and R_S are much smaller than bulk resistance R_L. Similarly, surface capacitance C_S is much smaller than bulk capacitor C_L.

In order to compute the SOC trajectory, we have adopted the following dynamics [15]

$$SOC(k+1) = SOC(k) - \frac{V_{oc} - \sqrt{V_{oc}^2 - 4(R_{int})T_m\cdot\omega_m\cdot\eta_m^{-sgn(T_m)}}}{2(R_{int})\cdot Q_b} \tag{4}$$

where, V_{oc} is the open circuit voltage of the battery, T_m is the electric motor torque, ω_m is the electric motor speed, η_m is electric motor efficiency, R_{int} is the internal resistance of the battery which is equivalent to R_L in the battery model in Fig. 1, Q_b is the battery capacity and SOC (k) is the state of charge at the k-th time instant. The SOC calculated with coulomb counting is the charging and discharging of the cells during a specified amount of time. Eq. (3) reveals that the SOC change depends on the operation mode and load demand. As the motor speed and motor torque increases the battery SOC drain increases. Typically, the healthy upper limits for battery SOC is 80–90%, while the healthy lower limits is about 20–30%. In this study, we have made a relatively conservative choice on the battery SOC range from 80% to 30% [16,17].

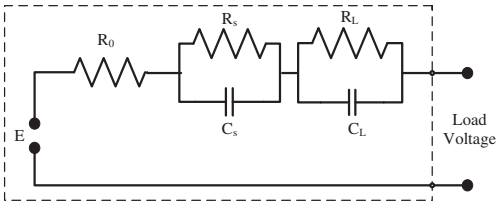

Fig. 1. Battery equivalent circuit.

3. Battery equalization

3.1. Battery equalization scheme

As the voltage in a single cell is quite low, for high voltage applications like EV, battery modules and packs are made via serial and parallel combinations of the cells [18]. Variations are inevitable in the internal resistances of the battery cells and modules. The variation in the internal resistance is caused by extrinsic or intrinsic cell properties, contact resistance among cells, or temperature gradient because of improper thermal management accounts for battery imbalance. The variation in the internal resistance causes variations in the SOC and degrades the cell [19]. The battery life can be significantly affected by the imbalance among modules or cells due to the associated over-charging or over-discharging. Hence, equalizing the modules or cells is important for acquiring the maximum achievable power and extending the battery life [20,21].

In this study, the voltage equalization scheme by Lee and Cheng is adopted [10], with a two-module situation shown in Fig. 2.The voltage of each module determines the direction of energy transfer between the two modules with proper operation of the MOSFET switches Q_1 and Q_2. L_1 and L_2 are two uncoupled inductors, while C_1 is an energy transferring capacitor.V_{B1} and V_{B2} are battery voltages for modules (or cells) 1 and 2, respectively. For normal condition, $V_{C1} = V_{B1} + V_{B2}$. The ideal condition is $V_{B1} = V_{B2}$, although this can seldom be the case in realistic operation.

With assistance of Fig. 3, two operational scenarios are described in the following. For the PWM operation, T_S is the period and D denotes the duty cycle.

1) $V_{B1} > V_{B2}$: For duration DT_S, Q_1 is turned on, and capacitor C_1transfers energy to V_{B2} during the same period inductor L_1 stores energy. For duration $(1 - DT_s)$, Q_1 is turned off, D_2 turns on, and the capacitor energy is supplied to Module #1 and L_2 charged by V_{B2}. In the switching duty cycle (T_s), as shown in Fig. 3, $T_1 - T_0 = DT_s$, while $T_2 - T_1 = (1 - DT_s)$. The operation can be described by the following equations.

a) For $t \in [T_0, T_1]$, Q_1 is turned on, which implies

$$V_{B1}(t) = L_1\frac{di_{L1}(t)}{dt} \quad \text{with} \quad i_{L1}(T)_0 = I_0 \tag{5}$$

$$V_{B2}(t) = -L_2\frac{di_{L2}}{dt} + \frac{1}{C_1}\int_{T_0}^{t} i_{L2}(\tau)d\tau \quad \text{with} \quad i_{L2}(T_0) = I_0 \tag{6}$$

b) For $t \in [T_1, T_2]$, Q_1 is turned off and Q_2 is turned on, which implies

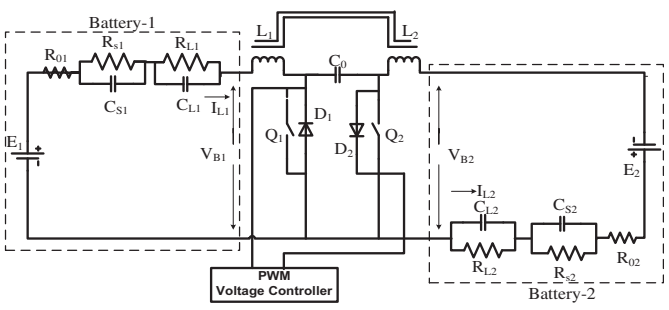

Fig. 2. Battery equalization circuit.

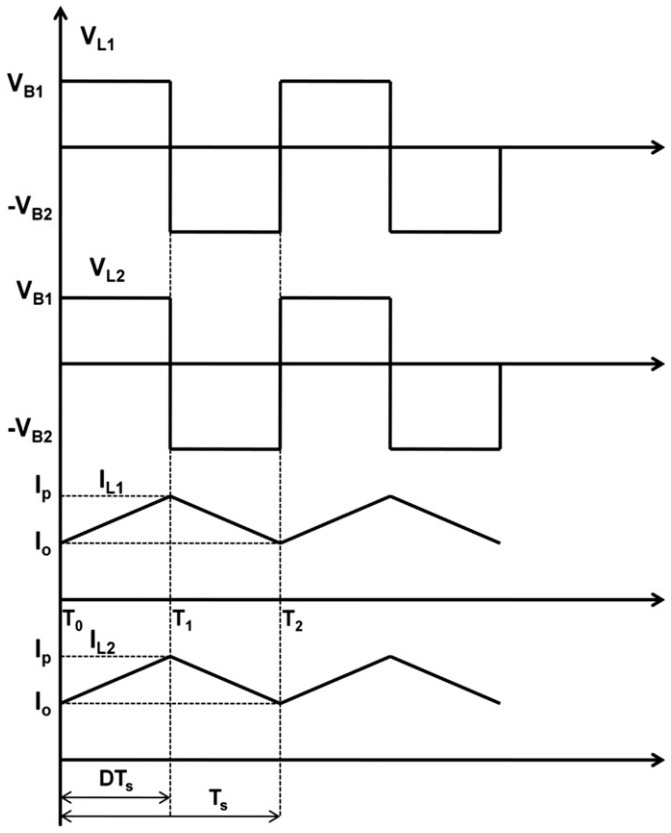

Fig. 3. Typical switching waveform of the battery equalizer when $V_{B1} > V_{B2}$.

$$V_{B1}(t) = L_1\frac{di_{L2}(t)}{dt} + \frac{1}{C_1}\int_{T_1}^{T_2} i_{L1}(\tau)d\tau \quad \text{with} \quad i_{L1}(T_1) = I_P \tag{7}$$

$$V_{B2}(t) = -L_2\frac{di_{L2}(t)}{dt} \quad \text{with} \quad i_{L2}(T_2) = I_P \tag{8}$$

Eqs. (4) through (7) describe voltages V_{B1} and V_{B2} dynamics during one duty cycle of PWM operation. I_p is the peak current during the operation cycle DT_s. The currents in the inductor I_{L1} and I_{L2} are given by

$$I_{L1} = \left[\frac{1}{2}\left(\frac{V_{B1}}{L_1}D^2 + \frac{V_{c1} - V_{B1}}{L_1}(1-D)^2\right)\right]T_s \tag{9}$$

$$I_{L2} = \left[\frac{1}{2}\left(\frac{V_{c1} - V_{B2}}{L_2}(1-D)^2 + \frac{V_{B2}}{L_2}(1-D)^2\right)\right]T_s \tag{10}$$

By varying the switching frequency, the equalization scheme can be implemented in continuous current or discontinuous inductor current mode. During the equalization process, the weak cell is charged by a strong cell to balance the energy level of both the cells. In our study battery 1 is at higher energy level than battery 2.

2) $V_{B1} < V_{B2}$: The operation is controlled by the switching Q_2 and D_1 in similar fashion as Case 1, and similar equations would apply.

3.2. Worthiness of replacement

The concept of worthiness of replacement (WOR) is applied to the battery pack after the battery is equalized and the trip is complete. As mentioned earlier though equalization is unavoidable but WOR projects the exact loss of energy in the trip. This analysis would be the decision making factor for projection of completion of the trip as the onboard energy is calculated. The WOR is defined as

$$\mathrm{WOR} = \left[\frac{\text{SOC Change of Current Battery Pack}}{\text{Battery Pack SOC Change with Certain Module(s) Replaced}}\right] \tag{11}$$

Eq. (10) can be enhanced by some averaging operation, for example for actual or predicted trips of certain number of days. Considering the stochastic factors in traffic conditions and driving behaviors, such averaging can help to obtain more reliable result for evolution purpose.

4. Subspace estimation of internal resistance MAP of EV battery pack

In order to obtain the module-wise internal resistance map of battery pack for WOR evaluation and online monitoring, we propose to estimate the internal resistance with the battery equalization signals, i.e. the associated voltage and current measurements, during the actual trip (i.e. with the driving cycle input).

In this study, the subspace identification [22] method is applied for the relevant parameter estimation based on the current and voltage measurements in the equalization circuit. Based on a state-space battery model, subspace parameter estimation permits estimation of static battery parameters based on input–output data (I_{in} and V_{o}). The process can be carried out online during the vehicle operation so that actual change of battery characteristics can be reflected [23].

The subspace identification theory is briefly reviewed in the following. For the m-input, p-output, n-th order system with discrete-time model

$$x(t+1) = Ax(t) + Bu(t) + w(t) \tag{12a}$$

$$y(t) = Cx(t) + Du(t) + v(t) \tag{12b}$$

where $x(t)$ are states, $u(t)$ and $y(t)$ are input and output, respectively, $w(t)$ is the process noise or disturbance, and $v(t)$ is the measurement noise. System (11) can be diagonalized via similarity transformation as

$$\tilde{x}(t+1) = T^{-1}AT\tilde{x}(t) + T^{-1}Bu(t) + \tilde{w}(t) \tag{13a}$$

$$y(t) = CT\tilde{x}(t) + Du(t) + v(t) \tag{13b}$$

where T is invertible and defined by

$$\tilde{x}(t) = T^{-1}x(t) \tag{14}$$

The output can be estimated by assuming that $\widehat{A}$ and $\widehat{C}$ are fixed, i.e.

$$y(t|B,D) = \widehat{C}\left(qI - \widehat{A}\right)^{-1}Bu(t) + Du(t) \tag{15}$$

is linear in B and D. The predictor is formed from past inputs, and Eq. (14) is an output error model. Therefore, if the system operates in open loop, one can consistently estimate B and D.

$$y(t|B,D,x_0) = \widehat{C}\left(qI - \widehat{A}\right)^{-1}x_0\delta(t) + \widehat{C}\left(qI - \widehat{A}\right)^{-1}Bu(t) + Du(t) \tag{16}$$

Eq. (15) is linear in $x_0 = x(0)$ and $\delta(t)$ is the unit pulse at time $t = 0$.

Matrices A and C are estimated from extended observability matrix for r observable rows, i.e.

$$G = \begin{pmatrix} C \\ CA \\ \vdots \\ CA^{r-1} \end{pmatrix} \tag{17}$$

G has dimensions $(pr) \times n$. C can be estimated by

$$\widehat{C} = G(1:p, 1:n) \tag{18}$$

Similarly, A is estimated by

$$G(p+1:pr, 1:n) = G(1:p(r-1), 1:n)\widehat{A} \tag{19}$$

After estimating the initial state, the prediction error minimization method can be used to determine the unknown parameters in the state-space model. In this study, the target parameter is the internal resistances for the respective batteries. The estimation quality can be evaluated with the prediction error

Fig. 4. Route map of the sample trip.

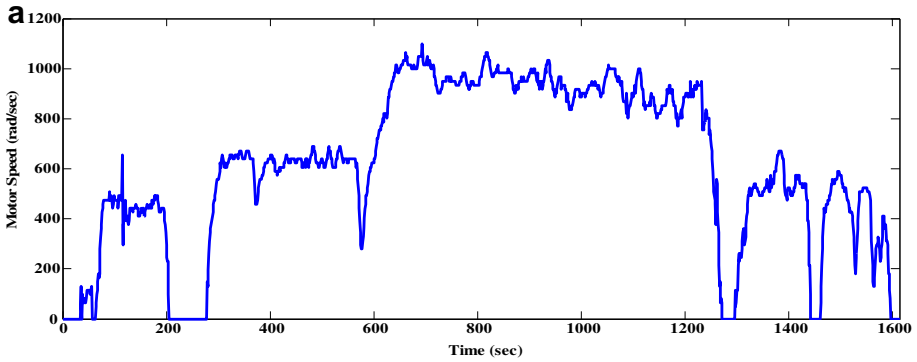

Motor speed during driving.

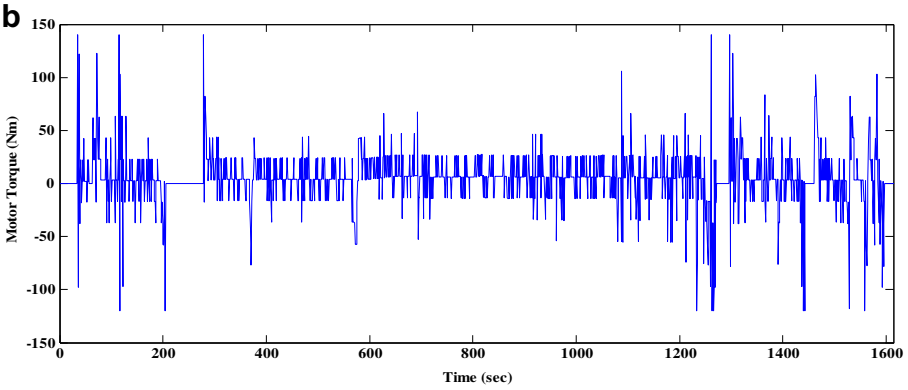

Motor torque profile during driving.

Fig. 5. Driving cycle and torque profile for the simulation example.

$$\varepsilon(t,\theta_*) = y(t) - \hat{y}(t|\theta_*) \tag{20}$$

for$1 \le t \le N$ the error sequence is filtered by

$$\varepsilon_F(t,\theta) = L(q)\varepsilon(t,\theta) \tag{21}$$

where, $L(q) \equiv 1$ in this case. For parameter estimation, the cost function is defined as

$$V_N\left(\theta, Z^N\right) = \frac{1}{N}\sum_{t=1}^{N} l[\varepsilon_F(t,\theta)] \tag{22}$$

where, $l(\cdot)$ is a quadratic function, $Z^N = [y(1),u(1),y(2),u(2),\cdots, y(N),u(N)]$ is the vector of the input–output data pairs. The least-square method is applied for parameter estimation:

$$\hat{\theta}_N = \hat{\theta}_N\left(Z^N\right) = \underset{\theta\in D_M}{\operatorname{argmin}}\ V_N\left(\theta, Z^N\right) \tag{23}$$

where, $\theta \in D_M \subset R^N$, and D_M is the set of parameter vectors. This procedure of estimating the required parameter θ is prediction-error identification method [22].

In order to apply the foregoing prediction-error identification method to battery equalization process, the associated state-space model is obtained as follows. Based on the two operational modes described in Section 3.1, the averaged state-space model was derived, as presented in the Appendix. When battery 1 is at higher energy level, battery 1 charges battery 2. Referred to Fig. 2, the averaged state-space model for battery 1 is

$$\begin{bmatrix}\dot{x}_1\\ \dot{x}_2\\ \dot{x}_3\\ \dot{x}_4\end{bmatrix} = \begin{bmatrix} -\frac{1}{R_{cs1}C_{cs1}} & 0 & \frac{1}{C_{cs1}} & 0\\ 0 & -\frac{1}{R_{cL1}C_{cl1}} & \frac{1}{C_{cL1}} & 0\\ \frac{-1}{L_1} & \frac{-1}{L_1} & \frac{-R_{01}}{L_1} & 0\\ 0 & 0 & \left(\frac{1}{C_0}-\frac{x}{C_0}\right) & 0\end{bmatrix}\begin{bmatrix}x_1\\ x_2\\ x_3\\ x_4\end{bmatrix} + \begin{bmatrix}0\\ 0\\ -\frac{x}{C_0}\\ 0\end{bmatrix} d \tag{24a}$$

$$E_1 = \begin{bmatrix}-2 & -2 & \frac{R_{01}}{L_1} & 0\end{bmatrix}\begin{bmatrix}x_1\\ x_2\\ x_3\\ x_4\end{bmatrix} \tag{24b}$$

where, x_1 is the voltage across capacitor C_{s1}, x_2 is the voltage across capacitor C_{L1}, x_3 is the current through inductor L_1, and x_4 is the voltage across capacitor C_0. Similarly, the state-space model for battery 2 is:

Table 1
Initial conditions of two-module simulation study.

Case no.	Battery no.	Voltage (V)	Capacity (Ah)	SOC (%)	Internal resistance (Ω)
1	B-1	100.8	20	80	0.075
	B-2	100.8	20	80	0.075
2	B-1	100.8	20	80	0.075
	B-2	100.8	20	65	0.30

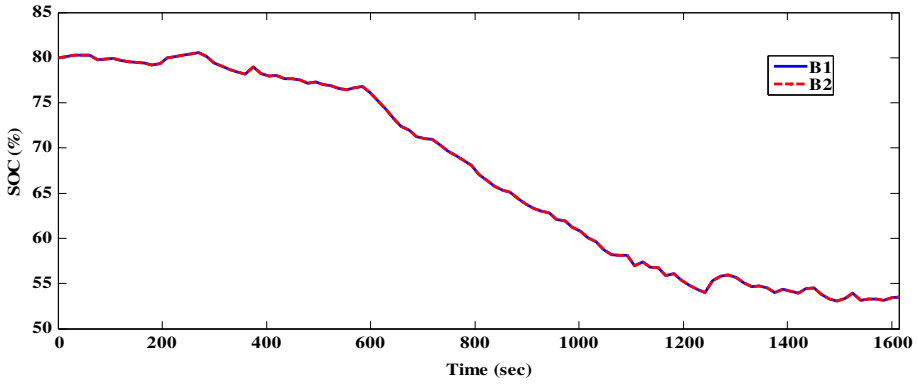

Fig. 6. Battery module SOC trajectories for with Case #1 with the example driving cycle.

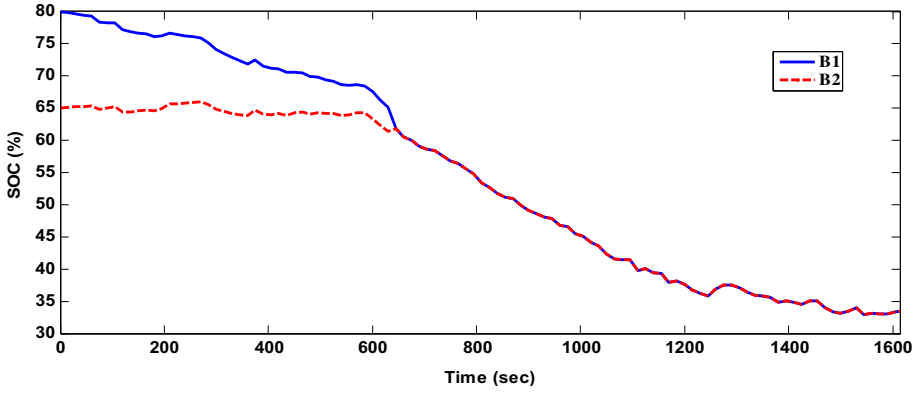

Fig. 7. Two-module battery SOC for example driving cycle for Case 2.

$$\begin{bmatrix}\dot{x}_1\\ \dot{x}_2\\ \dot{x}_3\\ \dot{x}_4\end{bmatrix} = \begin{bmatrix} -\frac{1}{R_{cs2}C_{cs2}} & 0 & \frac{1}{C_{cs2}} & 0\\ 0 & -\frac{1}{R_{cL2}C_{cL2}} & \frac{1}{C_{cL2}} & 0\\ \frac{-1}{L_2} & \frac{-1}{L_2} & \frac{-R_{02}}{L_2} & 0\\ 0 & 0 & \left(\frac{1}{C_0}-\frac{x}{C_0}\right) & 0 \end{bmatrix}\begin{bmatrix}x_1\\ x_2\\ x_3\\ x_4\end{bmatrix} + \begin{bmatrix}0\\ 0\\ -\frac{x}{C_0}\\ 0\end{bmatrix} d \tag{25a}$$

$$E_2 = \begin{bmatrix}-2 & -2 & \frac{R_{02}}{L_2} & 0\end{bmatrix}\begin{bmatrix}x_1\\ x_2\\ x_3\\ x_4\end{bmatrix} \tag{25b}$$

where, the states are same as those in Eq. (23).

After obtaining the values for the parameters from the subspace state-space estimation we calculate the values for each of the resistances. R_{CS1}, R_{CL1} and R_{01} are identified internal resistances for battery 1 and R_{CS2}, R_{CL2}, and R_{02} are internal resistances for battery 2. Thus the internal resistances of individual modules can be estimated throughout a specific trip.

5. Simulation results

Simulation study has been conducted to evaluate the proposed method. The driving cycle adopted is the one used in an earlier study [24], as shown in Fig. 4. The trip origin is 124 West Freistadt Road in Thiensville, while the destination is 3200 North Cramer Street in Milwaukee.

The proposed idea is evaluated with simulation study based on the EV model described in Section 2. The Matlab, Simulink and SimPowerSystem are used for the simulation. We used a lithium-ion battery model as a power source for the electric vehicle [12,13]. For the PMSM motor, the driving torque can be obtained by applying the driving cycle (speed profile) to the propulsion dynamics. The torque limits were set to 140 and −160 N m. The current limits for the battery side were set from 250 A to −250 A on the battery side. The driving cycle had both long and short segments of speeds [25]. The torque and speed profiles for the actual driving cycle are given in Fig. 5, which will later be used to simulate two and three module batteries with different cases. The concept of WOR in two different scenarios: a two-module battery pack first and then a three-module battery pack.

Table 2
Initial conditions of individual battery modules for simulation study.

Case no.	Battery no.	Voltage (V)	Capacity (Ah)	SOC (%)	Internal resistance (Ω)
1	B-1	64.8	20	80	0.054
	B-2	64.8	20	80	0.054
	B3	64.8	20	80	0.054
2	B-1	64.8	20	80	0.054
	B-2	64.8	20	72.5	0.081
	B-3	64.8	20	65	0.108
3	B-1	64.8	20	80	0.054
	B-2	64.8	20	80	0.081
	B-3	64.8	20	80	0.108

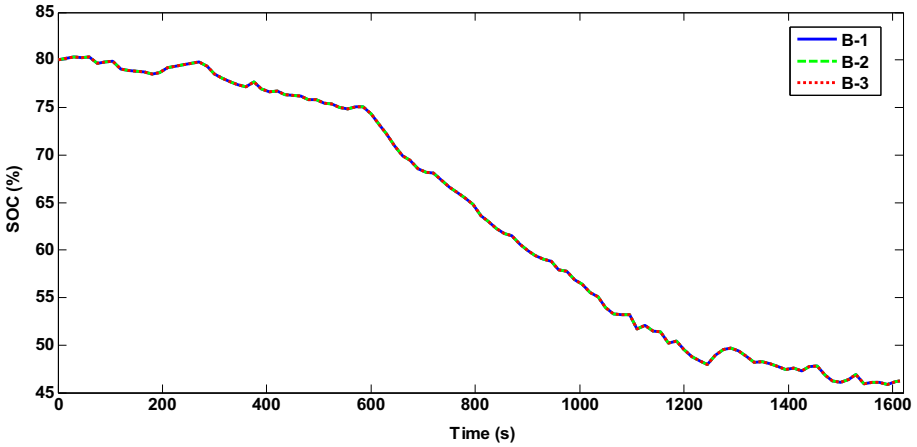

Fig. 8. SOC trajectory for Case 1 of three-module battery pack.

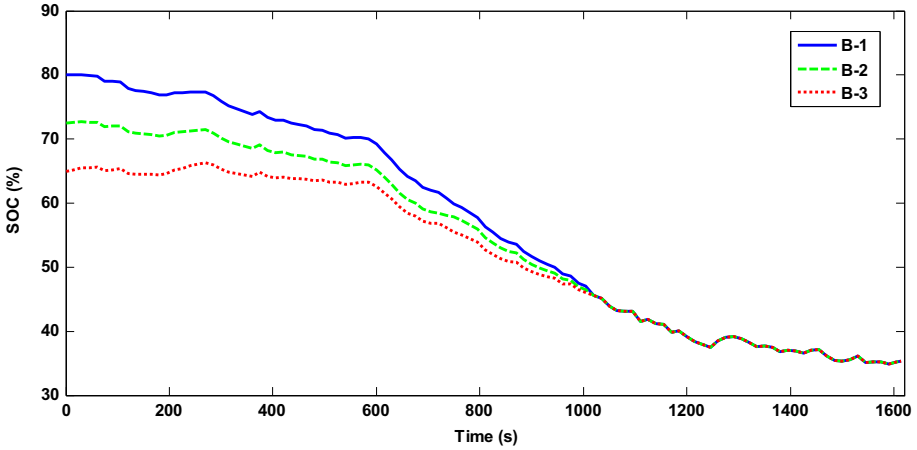

Fig. 9. Battery SOC trajectories for three modules for Case 2 of Table 2.

5.1. Simulation study for two-module battery pack

Two battery modules are assumed serially connected. For each module, the capacity rating is 20 Ah, respectively. The upper and lower limits of battery SOC are set to be 80% and 30%, respectively. Each module consists of 4 sub-modules which have 7 cells in series, i.e. 28 cells in total, with nominal voltage 3.6 V [26]. The voltage across the battery pack is 201.6 V [27], i.e. 100.8 V for each module.

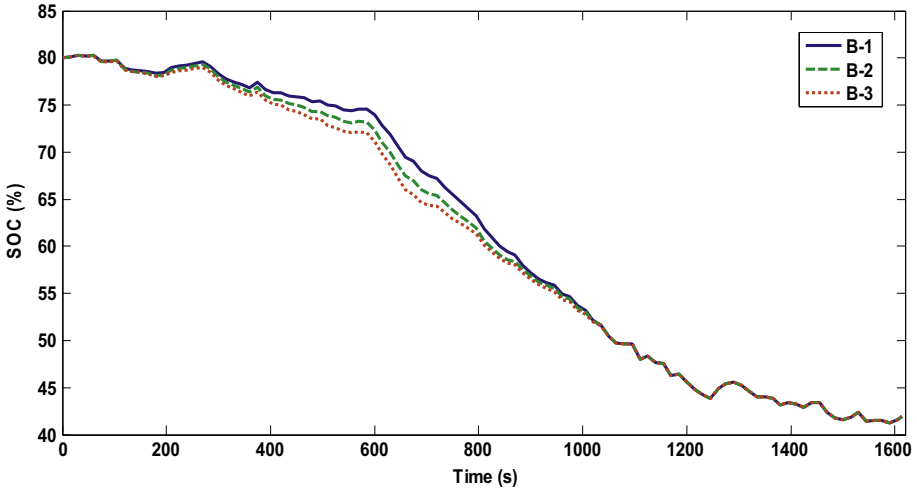

Fig. 10. Battery SOC trajectories for three modules for Case 2 for intermediate equalization.

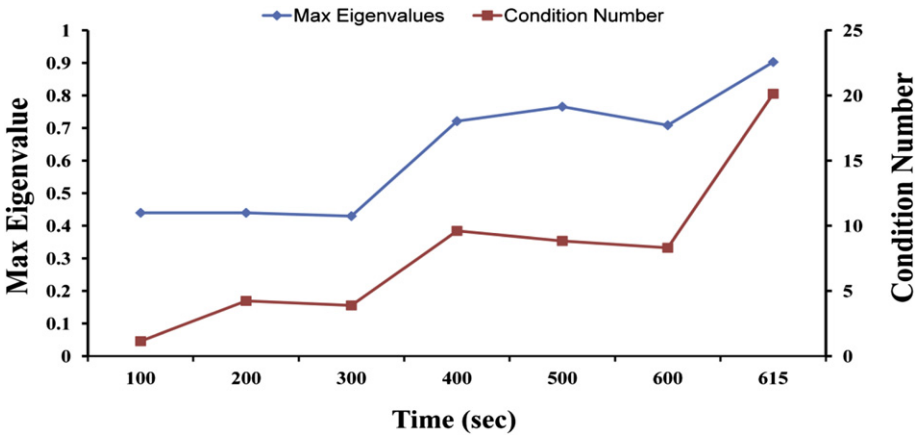

Fig. 11. Maximum eigen-value and condition number for the input signal throughout the trip.

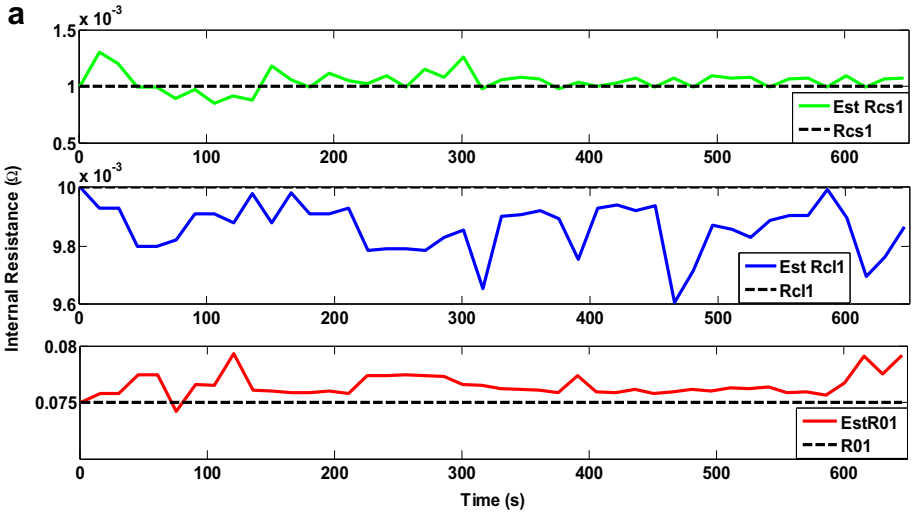

Battery module B-1

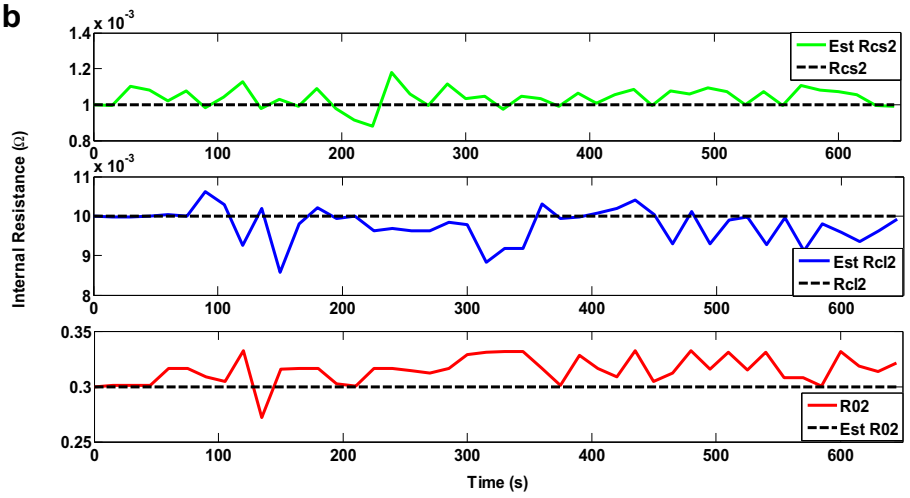

Battery module B-2

Fig. 12. Online estimation profiles for module-wise internal resistance for the 2-module case.

Two cases are simulated with the settings described below (also summarized in Table 1, with B-1 and B-2 representing battery modules 1 and 2, respectively):

Case 1 Both modules are in the nominal condition, i.e. having internal resistance of 0.075 Ω. Starting from 80% SOC, both modules follow the same discharging trajectory as shown in Fig. 6.The final SOC is 53.52%.

Case 2 Battery 1 is in nominal condition, while battery 2 is degraded with internal resistance of 0.30 Ω [28]. As battery 2 is degraded, we assume the starting SOC level is 65%. Such difference in SOC level results in the equalization process described earlier. In Fig. 7, we observe that the two modules equalize during the first 645 s of the driving cycles. The energy from B-1 charges B-2 to increase its SOC level. The two modules are equalized to 61.8% SOC, and then both modules discharged in identical fashion down to 33.45% SOC by the end of the driving cycle. Though the driving cycle is complete in Case 2 there is a considerable amount of energy loss from B-1 supplied to B-2 so as to equalize which could have been used for driving. For Case 2 in particular, it can be observed that, due to the relatively large internal resistance of B-2, there is significant amount of energy loss during the equalization from B-1 to B-2. The battery pack SOC changes by 26.48% in Case 1 (both modules healthy), while by 39.05% in Case 2. Such difference leads to the WOR of 1.47 for B-2.

5.2. Simulation study for three-module battery pack

Simulation is then performed for a battery pack with three modules in series. The capacity for each module is 20 Ah. The battery pack is composed of three modules. Each module consists of two serially connected sub-modules of nine cells each, i.e. 18 cells in series. This configuration results is 64.8 V across each module. The overall voltage across the battery pack is 194.4 V. The internal resistance for ideal module is assumed to be 0.054 Ω.

Three cases are simulated, with settings listed in Table 2, with B-1, B-2 and B-3 standing for battery modules 1, 2 and 3, respectively. For Case 1, all the modules are in nominal condition, i.e. with internal resistance of 0.075 Ω and 80% initial SOC. For Case 2, B-1 is in nominal condition, B-2 has internal resistance of 0.15 Ω with 72.5% initial SOC, and B-3 has internal resistance of 0.3 Ω with 65% initial SOC. This case is intended to make B-2 and B-3 more degraded modules. Case 3 is similar to case 2 except that the starting SOC is identically at 80%.

For Case 1, all the modules demonstrate identical discharging trajectories as shown in Fig. 8, with the final SOC of 46.26%. In Case 2, as shown in Table 2, B-1, B-2, and B-3 have different initial SOC levels, which results in equalization among the three modules from the start till 1005 s, as shown in Fig. 9. In particular, B-1 has higher SOC than B-2, and B-2 has higher SOC than B-3. The equalization of these three battery modules follows the same logic as described earlier, i.e. the equalization decision is made for every pair of neighboring modules based on the comparison of the relevant voltages, which is done by triggering the associated switches. In the scenario assumed

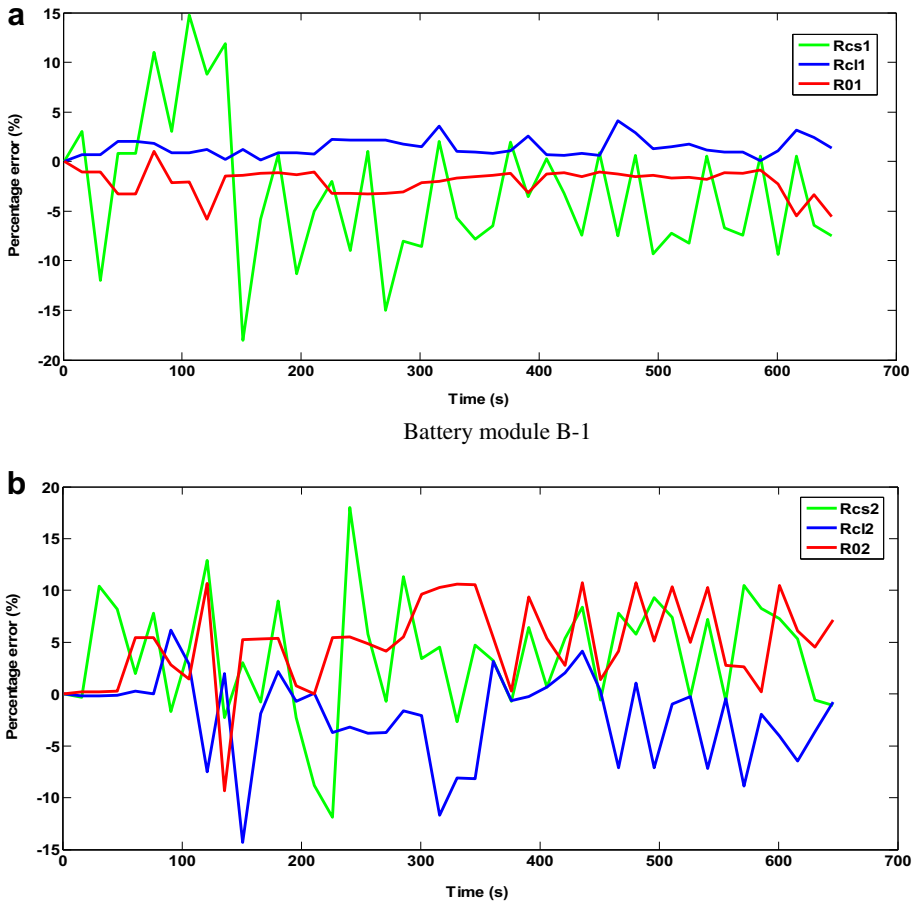

Fig. 13. Relative error in estimating module internal resistance for the two-module case.

for Case 2, current is discharged from B-1 to B-2, and current is discharged from B-2 into B-3. All the modules equalize their SOC to 45.57%. Afterwards, the three modules jointly discharge to 35.34% SOC by the end of the driving cycle. Although, in Case 2, the driving cycle can be completed with the onboard battery power, there is a considerable amount of SOC from B-1 supplied to B-2, and that from B-2 supplied to B-3. Further, more, due to the relatively higher internal resistances of B-2 and B-3, there is significant amount of energy loss during the aforementioned equalization processes. To complete the same trip, the average SOC drops by 33.74% in Case 1, while in Case 2, by 37.16%. The corresponding WOR is 1.102.

Simulation has also been performed to the situation when battery module equalization occurs not from the start of the trip, but rather in the middle of the trip as the SOC difference increases. For this purpose, we consider the same battery configuration as in Table 2, while all the modules have equal starting SOC, i.e. 80%. The SOC deviates for each module during the first 645 s, and thenafter the equalization process starts. As shown in Fig. 10, the SOC

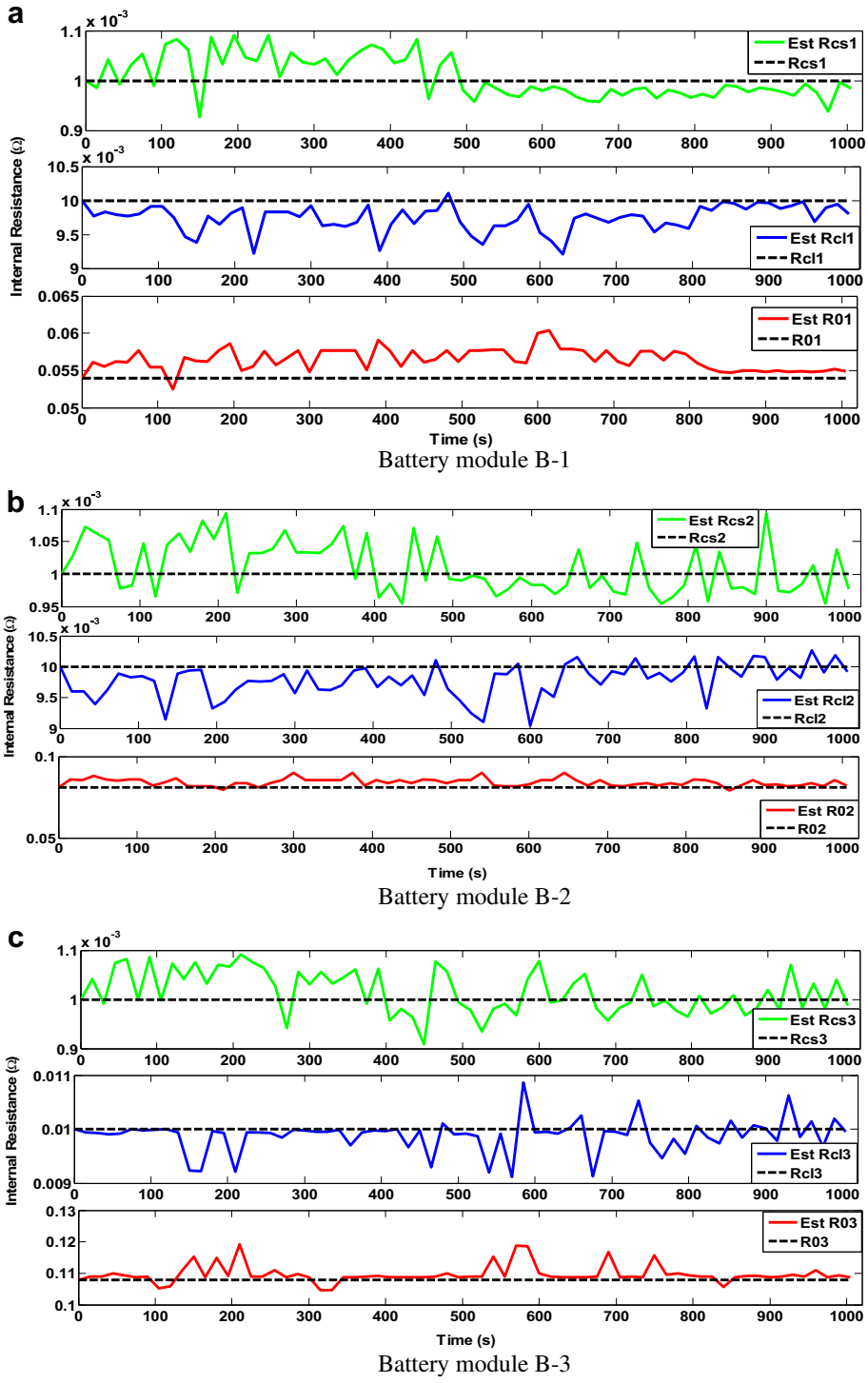

Fig. 14. Estimation of battery module internal resistances for the 3-module case.

difference between battery 1 and battery 2 was 2.05% and that between battery 2 and battery 3 was 1.53%, respectively. With the equalization process, the modules are equalized to 50.45% by 1050 s. Then the whole battery pack completes the driving cycle at SOC 41.95%. The total energy required to travel the trip was 38.05%, and the WOR was 1.105 in this case.

The above simulation results show that equalization can handle the presence of degraded module during vehicle's operation however there is a considerable amount of SOC loss during equalization. Highly degraded modules have significantly high internal resistance, which would waste the battery energy and in turn lead to uneconomical operation. If the module-specific internal resistance can be identified online, the vehicle owners can perform the economical analysis based on their preferred trips, and make reasonable decision on module replacement.

5.3. Subspace parameter estimation

The subspace identification scheme described in Section 4 is applied to the two-module case for estimating the battery internal resistances. As described earlier in battery modeling section, there are surface internal resistance, load resistance and terminal resistance that appear in the state-space model of battery equalization. This study mainly considers the following parameters: surface capacitance (C_s), bulk capacitance (C_l), inductors (L_1 and L_2) in the equalization circuit, capacitors (C_0) from the equalization circuit, surface internal resistance R_s, and bulk internal resistance R_l. The nominal values for the capacitance and inductance parameters in the two-module simulation case are set as: $C_l = 90000$ F, $C_s = 9000$ F, $L_1 = L_2 = 13$ mH and $C_0 = 12$ μF.

In order to assure the unique solution or convergence of the parameter estimation, the condition of persistent excitation (PE) is evaluated for the input signals [29]. The PE order of is n if

$$C_n = \lim_{t\to\infty} \frac{1}{t}\varphi^T\varphi = \begin{bmatrix} c(0) & c(1) & \cdots c(n-1) \\ c(1) & c(0) & \cdots c(n-2) \\ \vdots & & \\ c(n-1) & c(n-2) & \cdots c(0) \end{bmatrix} \quad (26)$$

is nonsingular, where the covariance of input is given by

$$c(k) = \lim_{t\to\infty} \frac{1}{t}\sum_{i=1}^{t} u(i)u(i-k) \quad (27)$$

Determination of PE order is based on the evaluation of the covariance matrix and check if it is full rank. The number of parameters to be estimated should not higher than the order of PE that can be achieved for the given input–output data. Using eigenvalues is a more reliable method to check the matrix singularity. The condition number, i.e. the ratio of the largest eigen-value magnitude to the smallest, is a more trustable index to just if a matrix is full rank even though all eigen-values are non-zero. If the condition number is very large, the full rank condition is not practically valid.

In this study, the input is the duty ratio of the equalization circuit. The input data segment for every 100 s is used to evaluate if the 4th order PE is valid. The condition numbers and the maximum magnitude eigen-values shown in Fig. 11 validate the 4th order PE condition.

The internal resistances for Battery B-1 (R_{cs1}, R_{cl1} and R_{01}) and Battery B-2 (R_{cs2}, R_{cl2} and R_{02}) are estimated using the subspace identification method described earlier. The online estimation of the internal resistances of B-1 and B-2 are shown in Fig. 12. The relative errors in estimating the internal resistances are plotted in Fig. 13, which are within 18%. Such accuracy is generally acceptable for fault detection and WOR evaluation purpose. Notice that the estimation error for R_0 is relatively smaller, while that for R_{cs} is relatively larger.

Similar simulation study is then performed for the 3-module equalization process. In this case, the parameters we identify are R_{cs1}, R_{cl1} and R_{01} for Battery B-1, R_{cs2}, R_{cl2} and R_{02} for Battery B-2, and R_{cs3}, R_{cl3} and R_{03} for Battery B-3, respectively. The parameters R_{cs} and R_{cl} are 0.001 Ω and 0.01 Ω whereas $R_{01} = 0.054$ Ω, $R_{02} = 0.081$ Ω and $R_{03} = 0.108$ Ω. The three plots in Fig. 14 show the estimation results for the internal resistances for each of the three battery modules, respectively. Fig. 15 shows the relative errors for these estimations. For Battery B-1, R_{cs1} has mean deviation of 0.8% with variation from −7.8–9.25%, R_{cl1} has a mean deviation of −2.5% with a variation from −7.8 to 1% and R_{01} has mean deviation of 4.5% with variation from −2.75–11.75%. For Battery B-2, R_{cs2} has mean deviation of 1% with variation from −4.6–9.4%, R_{cl2} has a mean deviation of −2.2% with a variation from −9.6 to 2.66 %, and R_{02} has mean deviation 3.9% with variation from −2.4–11.15%. For Battery B-3, R_{cs3} has mean deviation of 1.7% with variation from −8.9–9.32%, R_{cl3} has a mean deviation of −1.15% with a variation from −8.6–8.8% and R_{03} has mean deviation of 1.6% with variation from −3.0–10.45%. For all cases, the relative errors of

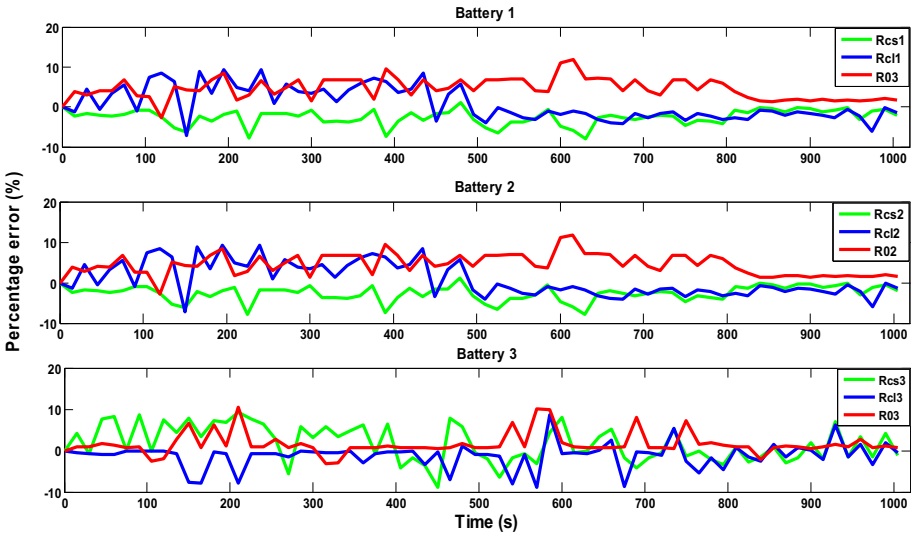

Fig. 15. Relative error in estimating battery module internal resistance for the 3-module case.

estimation are bounded by 11.75%, which is again acceptable for degradation evaluation purpose.

6. Conclusion

This paper presents two ideas around the non-uniform degradation of battery pack for electric vehicles. First, the internal resistance of each individual module is estimated online during vehicle operation using the battery equalization signals. A subspace identification method is adopted for such purpose. Second, after the module-wise internal resistance map is obtained, the trip specific WOR can be evaluated, which indicates both the energy lost due to high internal resistance of certain module and the potential performance recovery if a healthy module can be installed. Simulation study has been performed using an actual driving cycle for a commuting trip. The identification of the internal resistances demonstrated less than 18% relative error, which is acceptable performance. As battery module replacement is a big issue for EV maintenance, the proposed ideas provide a convenient way to onboard health map identification, along with a quantitative measure for evaluating the necessity of replacement for certain module.

Appendix. Battery equalization model derivation

The schematic diagram for the battery equalization circuit is shown in Fig. 2. Fig. A.1 shows the circuit diagram for battery 1 when switch Q_1 is in on state.

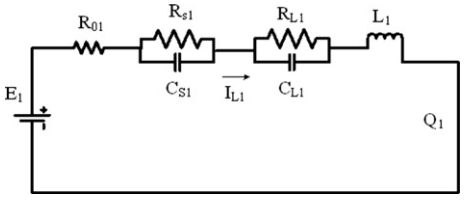

Fig. A.1. Equivalent circuit diagram for battery equalization when Q_1 is on.

The relevant dynamics can be modeled as:

$$\dot{V}_{cs1} = \frac{1}{C_{cs1}} i_{L1} - \frac{1}{R_{cs1}C_{cs1}} V_{cs1} \tag{A.1a}$$

$$\dot{V}_{cL1} = \frac{1}{C_{cL1}} i_{L1} - \frac{1}{R_{cL1}C_{cL1}} V_{cs1} \tag{A.1b}$$

$$\dot{i}_{L1} = \frac{R_{01}}{L_1} i_{L1} - \frac{1}{L_1} V_{cs1} - \frac{1}{L_1} V_{cL1} \tag{A.1c}$$

$$\dot{V}_0 = \frac{1}{C_0} i_{L1} \tag{A.1d}$$

The circuit diagram for battery 1 when switch Q_1 is in off state is shown in Fig. A.2, for which the associated dynamics can be modeled as

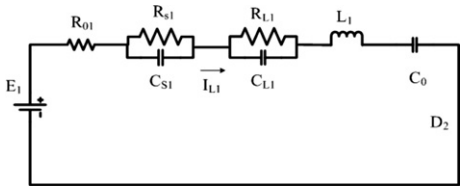

Fig. A.2. Circuit diagram for equalization process when switch Q_1 is off.

$$\dot{V}_{cs1} = \frac{1}{C_{cs1}} i_{L1} - \frac{1}{R_{cs1}C_{cs1}} V_{cs1} \tag{A.2a}$$

$$\dot{V}_{cL1} = \frac{1}{C_{cL1}} i_{L1} - \frac{1}{R_{cL1}C_{cL1}} V_{cs1} \tag{A.2b}$$

$$\dot{i}_{L1} = \frac{R_{01}}{L_1} i_{L1} - \frac{1}{L_1} V_{cs1} - \frac{1}{L_1} V_{cL1} \tag{A.2c}$$

$$\dot{V}_0 = \frac{1}{C_0} i_{L1} \tag{A.2d}$$

If the duty ratio of the circuit switch is denoted by d, an averaged model can be obtained by combining Eqs. (A.1) and (A.2), i.e.

$$\dot{V}_{cs1} = \frac{1}{C_{cs1}} i_{L1} - \frac{1}{R_{cs1}C_{cs1}} V_{cs1} \tag{A.3a}$$

$$\dot{V}_{cL1} = \frac{1}{C_{cL1}} i_{L1} - \frac{1}{R_{cL1}C_{cL1}} V_{cs1} \tag{A.3b}$$

$$\dot{i}_{L1} = \frac{R_{01}}{L_1} i_{L1} - \frac{1}{L_1} V_{cs1} - \frac{1}{L_1} V_{cL1} \tag{A.3c}$$

$$\dot{V}_0 = \left(\frac{1}{C_0} - \frac{x}{C_0}\right) i_{L1} - \frac{x}{C_0}\delta \tag{A.3d}$$

where, x is constant operating current. Similar derivation can be performed for battery 2 with on and off positions for switch Q_1.

References

[1] C.-C. Chan, A. Bouscayrol, K. Chen, Electric, hybrid and fuel-cell vehicles architecture and modeling, IEEE Transactions on Vehicular Technology 59 (2) (2010) 589–598.
[2] A. Affani, A. Bellini, G. Franceschini, P. Guglielmi, C. Tassoni, Battery choice and management for new generation electric vehicles, IEEE Transactions on Industrial Electronics 52 (5) (2005) 1343–1349.
[3] P.A. Cassani, S.A. Williamson, Feasibility analysis of a novel cell equalizer topology for plug-in hybrid electric vehicle energy-storage systems, IEEE Transactions on Vehicular Technology 58 (8) (2009) 3938–3946.
[4] H.S. Park, C.H. Kim, K.B. Park, G.W. Moon, J.H. Lee, Design of charge equalizer based on battery modularization, IEEE Transactions on Vehicular Technology 58 (7) (2009) 3216–3222.
[5] M. Dubarry, N. Vuillaume, B.Y. Law, From single cell model to battery pack simulation for Li-ion batteries, Journal of Power Sources 186 (2009) 500–507.
[6] R. Ugle, Y. Li, Trip specific evaluation of worthiness of replacement of individual cells for battery pack in electric vehicles. SAE Paper No. 2011-01-1361, SAE 2011 World Congress and Exhibition (April 2011). Detroit, MI, USA.
[7] M. Einhorn, W. Roesseler, Improved performance of serially connected Li-ion batteries with active cell balancing electric vehicles, IEEE Transactions on Vehicular Technology 60 (6) (2011) 2448–2457.
[8] C.F. Chiasserini, R. Rao, Improving battery performance by using traffic shaping techniques, IEEE Journal on Selected Area of Communications 19 (7) (2001) 1385–1394.
[9] Z.-R. Peng, M.-H. Tsou, Internet GIS: Distributed Geographic Information Services for the Internet and Wireless Network, Wiley, Hoboken, NJ, 2003.
[10] Y.-S. Lee, M.-W. Cheng, Intelligent control battery equalization for series connected lithium-ion battery strings, IEEE Transactions On Industrial Electronics 21 (5) (2005) 1213–1223.
[11] B. McQueen, J. McQueen, Intelligent Transportation Systems Architectures, Artech House, Norwood MA, 2003.
[12] C.M. Shepherd, Design of primary and secondary cells – part 2. An equation describing battery discharge, Journal of Electrochemical Society 112 (July 1965) 657–664.
[13] Tremblay O., Dessaint L.-A., Dekkiche A.-I., A generic battery model for the dynamic simulation of hybrid electric vehicles, Proc. IEEE Vehicle Power and Propulsion Conference, 2007, pp. 284–289, Sept. 9–12.
[14] L. Gao, S. Liu, R.A. Dougal, Dynamic lithium-ion battery model for system simulation, IEEE Transactions on Components and Packaging Technologies 25 (3) (2002) 495–505.
[15] J. Larminie, J. Lowry, Electric Vehicle Technology Explained, John Wiley &Sons, 2003.

[16] L. Benni, D. Bruni, A. Macii, E. Macii, M. Poncino, Discharge current steering for battery life time optimization, IEEE Transactions on Computers 52 (8) (2003) 985–995.
[17] S. Kim, A novel state of charge estimation method for lithium-ion battery using sliding mode observer, Journal of Power Sources 163 (2006) 584–590.
[18] X. Hu, F. Sun, Y. Zou, Estimation of state of charge of a lithium-ion battery pack for electric vehicles using an adaptive Luenberger observer, Energies 3 (2010) 1586–1603.
[19] S. Lee, J.-H. Kim, J.-M. Lee, B.-H. Cho, State-of-charge and capacity estimation of lithium-ion battery using a new open-circuit voltage versus state-of-charge, Journal of Power Sources 185 (2008) 1367–1373.
[20] Y.-S. Lee, G.-T. Cheng, Quasi-resonant zero-current-switching bidirectional converter for battery equalization applications, IEEE Transactions on Power Electronics 21 (5) (2006) 1213–1223.
[21] T.A. Stuart, W. Zhu, A targeted equalizer for lithium-ion battery packs, Proc. 5th IEEE Vehicle Power and Propulsion Conference, pp. 207–212, 2009.
[22] L. Ljung, System Identification Theory for the User, second ed., Prentice Hall, 1998.
[23] J.-N. Juang, Applied System Identification, Prentice Hall, 1994.
[24] Q. Gong, Y. Li, Z.-R. Peng, Trip based optimal power management of plug-in hybrid electric vehicles with advanced traffic modeling, SAE International Journal on Engines 1 (1) (2009) 861–872.
[25] Q. Gong, Y. Li, Z.-R. Peng, Trip based optimal power management of plug-in hybrid vehicles, IEEE Transactions on Vehicular Technology 57 (6) (2008) 3393–3401.
[26] M. Dubarry, N. Vuillaume, B.-Y. Liaw, Origins and accommodation of cell variations in Li-ion battery pack modelling, International Journal of Energy Research 34 (2) (2009) 216–231.
[27] C. Sen, N.C. Kar, Battery pack modeling for the analysis of battery management system of a hybrid electric vehicle, Proc. 5th IEEE Vehicle Power and Propulsion Conference, pp. 207–212, 2009.
[28] A. Vasebi, S.M.T. Bathaee, M. Partovibaksh, Predicting state of charge of lead acid batteries for hybrid electric vehichles, Energy Conversion and Management 49 (2008) 75–82.
[29] K.J. Aström, B. Wittenmark, Adaptive Control, second ed., Prentice Hall, 1994.